JOURNAL OF MATERIALS SCIENCE 19 (1984) 1077–1088

The preparation and characterization of alumina membranes with ultra-fine pores

Part 1 *Microstructural investigations on non-supported membranes*

A. F. M. LEENAARS, K. KEIZER, A. J. BURGGRAAF
Twente University of Technology, Department of Chemical Engineering, Laboratory for Inorganic Chemistry and Materials Science, P.O. Box 217, 7500 AE Enschede, The Netherlands

Alumina films less than 20 μm thick are prepared by a process in which a boehmite sol is successively gelled, dried and calcined. The resulting structure has the unique property that only ultra-fine pores with a narrow pore size distribution are present within large crack-free layers. The microstructure can be influenced by the sintering temperature and the acid concentration of the precursor sol. The minimum modal pore size which has been obtained is 2.5 nm. A consistent model of the microstructure of the membranes and an explanation of its uniformity are presented.

1. Introduction

The use of membranes for separation purposes is becoming increasingly important. Water desalination, ultrafiltration processes in the food industry and in waste water treatment, and separation of gas mixtures are just a few examples of the use of membranes in large scale processes. A state of the art review and future prospects concerning the use of organic membranes have been presented recently [1]. A review of inorganic membranes has been written by the present authors [2]. It shows that only a few types of inorganic membranes are available commercially. It appears to be very difficult to prepare crack-free inorganic films with ultrafine pores *and* a narrow pore size distribution. Membranes with a narrow pore size distribution, in which especially large pores should be absent, are necessary to obtain a high degree of separation of mixtures. The modal pore size required depends on the type of mixture to be separated. The thickness of the membrane should be small enough to obtain a flux which is sufficiently high to make the process economically feasible. The use of inorganic instead of organic membranes is advantageous if one is dealing with high temperatures, aggressive mixtures (chemical, mechanical, microbiological), high pressures (no compaction of inorganic membranes) or separation circumstances which make frequent cleaning of the membrane necessary.

The microstructure of ultrafine ceramic compacts in different stages of processing (pressing, sintering) has been investigated thoroughly in our laboratory [3–5]. It has been found that the preparation of ultrafine grained ceramics with a high density is possible, when a ceramic compact consisting essentially of very fine crystallites and having small pores and a narrow pore size distribution is used as a starting material for the sintering process. This narrow pore size distribution is obtained as a result of a regular particle stacking. The concept of regular particle stacking achieved from sols instead of powders is the basis of this work.

A major obstacle in the preparation of fired ceramic bodies directly from sols and without the use of binders is the loss of coherency of the body during drying and firing. Yoldas [6, 7] claims that such a preparation for *bulk* ceramic bodies should be possible when a boehmite sol is used as a precursor. A crystal size of 6.9 nm, a pore size of 7.8 nm (assuming cylindrical pores) and a porosity

0022–2461/84 $03.00 + .12

of 65% are reported after sintering at 500° C. It will be shown that considerably lower pore sizes combined with somewhat lower porosities can be achieved for thin films. Arguments for selecting boehmite for our investigations are that the system is chemically relatively simple while its microstructure is very flexible. Furthermore, γ-AlOOH (boehmite) and its conversion to so-called transition aluminas have been widely investigated [8–11], which makes a proper choice of preparation conditions somewhat easier.

Thin films used in separation processes with a pressure gradient have to be supported by a porous carrier. However, the interpretation of experimental results of non-supported membranes is more straightforward than that of supported membranes, where the effects due to membrane and support have to be separated. Because the preparation of supported and non-supported membranes proceeds in a comparable way (see Fig. 1), the results obtained from non-supported films are expected to be applicable to supported films. This statement will be proved in Section 3.4. Therefore the research for finding a procedure for the preparation of supported thin films and the investigation of non-supported films has been carried out simultaneously. The latter have then been used for a thorough investigation of the microstructural development as a function of preparation conditions.

2. Experimental details

Boehmite (γ-AlOOH) sols were prepared by adding aluminium secondary butoxide to water which was heated to a temperature above 80° C and stirred at high speed. Two litres of water were used per mol of alkoxide. The solution was kept at 90° C and, about $\frac{1}{2}$ to 1 h after addition of the alkoxide, 0.07 mol HNO_3 per mol alkoxide was added to peptize the sol particles unless stated otherwise. The sol was kept boiling in the open reactor for a few hours to evaporate most of the butanol and was subsequently kept at 90 to 100° C during about 16 h under reflux conditions. The gels prepared according to Section 3.1 were calcined at a rate of $10^\circ\,C\,h^{-1}$ and kept at the final temperature for 34 h.

X-ray diffraction studies were carried out with a Philips X-ray diffractometer PW 1370 with nickel filtered Cu$K\alpha$ radiation. The pore size analyses were performed with a Carlo Erba Mercury porosimeter (200 series) and a Carlo Erba Sorptomatic (1800 series) for gas adsorption–desorption studies, using N_2 at 77 K. Transmission electron microscopy (TEM) was performed with a Jeol 200 CT instrument.

3. Results

3.1. Preliminary investigations

When boehmite sols are concentrated by drying, they are converted into gels. It appears that gel films dried at room temperature and relative humidities of 40 to 80% form cracks when their thickness is larger than roughly 20 μm after drying, the exact thickness limit being a function of process conditions. Another condition that should be fulfilled in order to acquire crack-free films is that the carrier surface should be well wetted by the sol.

The following procedure was adopted to obtain non-supported calcined films (see Fig. 1). A ceramic support is coated with a cellulose acetate film. A quantity of sol is poured onto this film so that the layer thickness after calcination is about 20 μm. After drying, the resulting gel is placed in acetone to dissolve the cellulose acetate and to obtain the non-supported gel film, which can then be calcined. The preparation scheme of supported gel films contains the same general steps, though the processing between steps 2 and 4 (see Fig. 1) is carried out differently. A detailed description will be presented elsewhere.

3.2. The influence of temperature treatment on the microstructure

A series of membranes were prepared containing 0.07 mol HNO_3 per mol of γ-AlOOH. In Table I the temperature treatments given and the resulting phases acquired, as measured by X-ray diffraction, are presented. The transition of γ-AlOOH to γ-Al_2O_3 takes place at about 390° C as shown by high temperature Guinier X-ray diffraction. The diffraction peaks of all samples other than the sample heated to 1000° C are very broad. The intrinsic (i.e. corrected) integral line width is between 1.5° and 3.8°. Because of these broad reflections no distinction can be made between γ-Al_2O_3 and δ-Al_2O_3. Moreover, only the [1 2 0] and [0 3 1] reflections of boehmite and the [4 0 0] and [4 4 0] reflections of γ/δ-Al_2O_3 can be used for the determination of the crystallite size by X-ray line-broadening measurements. The crystallite size was calculated according to Klug and Alexander [12]. A small tetragonal distortion

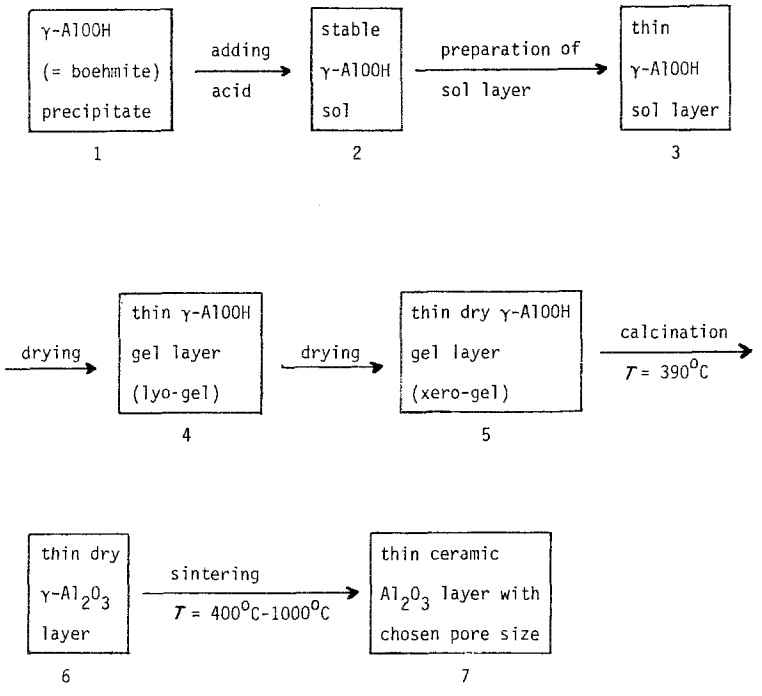

Figure 1 Flow diagram of the preparation of alumina membranes.

TABLE I Microstructural characteristics of membranes as a function of temperature treatment

Temperature (°C)	Phase	D^*_{hkl} (nm)	BET surface ($m^2\ g^{-1}$)	Modal pore size (nm)		Porosity (%)
				Cylindrical shaped	Slit-shaped	
200	γ-AlOOH	$D_{120} = 6.2$ $D_{031} = 4.8$	315 ± 2	3.7	2.5	41
400	γ/δ-Al_2O_3	$D_{400} = 6.4$ $D_{440} = 3.0$	301 ± 7	4.0	2.7	53
500	γ/δ-Al_2O_3	$D_{400} = 6.7$ $D_{440} = 6.5$	240 ± 1	4.9	3.2	54
600	γ/δ-Al_2O_3	$D_{400} = 6.6$ $D_{440} = 3.9$	209 ± 1	5.5	3.5	55
700	γ/δ-Al_2O_3	$D_{400} = 5.8$ $D_{440} = 5.2$	181 ± 1	5.9	3.7	53
800	γ/δ-Al_2O_3	$D_{400} = 6.1$ $D_{440} = 4.5$	154 ± 2	7.9	4.8	55
900	θ-Al_2O_3 (γ/δ-Al_2O_3)	–	99 ± 2	8.9	5.4	48
1000	α-Al_2O_3 (θ-Al_2O_3?)	$D_{012} = 65.2$ $D_{104} = 44.6$	15 ± 3	78	39	41
300†	γ-AlOOH	$D_{120} = 14.5$ $D_{031} = 12.3$ $D_{080} = 6.4$	131 ± 1	9.3	5.6	47
550†	γ/δ-Al_2O_3	$D_{400} = 5.7$ $D_{440} = 6.2$	147 ± 4	10.2	6.1	59

*Crystallite size measured in *h k l* direction through the crystallite.
†Prepared from sol obtained by autoclave treatment.

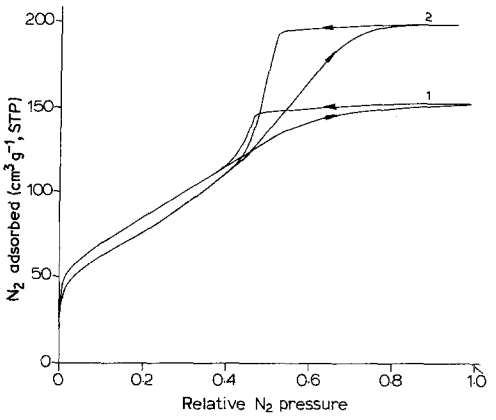

Figure 2 Gas adsorption–desorption isotherms of boehmite membranes (1), and of γ-Al_2O_3 membranes calcined at 400° C (2).

occurs in the γ/δ-Al_2O_3 phase, which is measured quantitatively by Wilson as a function of temperature [11]. Because Wilson used large boehmite crystals as a precursor material whereas our boehmite samples consist of very small crystals, the distortion will probably be different in both cases. Therefore the correction factors were not applied to our samples and consequently the values for the crystallite size of the oxidic phases might be rather inaccurate. The crystallite sizes found in this way are comparable with those found by electron microscopic measurements (see Section 4.2.2).

Mercury porosimetry applied to a sample calcined at 500° C shows that no pores with a size larger than 8 nm are present, assuming a contact angle of 140° between mercury and the solid surface (as valid for most solid materials) and a cylindrical pore shape. Pores smaller than about 50 nm can be detected by the gas adsorption–desorption technique [13]. The isotherms of the samples heated to 200° C and 400° C are shown in Fig. 2. A pore size distribution curve is calculated from the desorption isotherms, applying the Kelvin equation and assuming cylindrical pores (Fig. 3a) or slit shaped pores (Fig. 3b). In both cases the adsorbed layer thickness as given by Halsey's equation is used [13], which closely corresponds to the values measured by Lippens *et al.* [14] for aluminium hydroxides and oxides. In Section 4.2 the question of which pore shape is preferable is discussed on the basis of the data available. The modal pore sizes of the samples are given in Table I. The pore size distribution curves show that pores about 0.3 nm larger than the modal pore size are not observed for all samples. From the initial part of the adsorption isotherms the BET surface areas were calculated, taking 0.162 nm^2 as the area occupied per adsorbed N_2 molecule [13].

According to Gurvitsch's rule [13] all pores are supposed to be filled with liquid nitrogen at a relative pressure of 0.95. Taking 0.808 $g\,cm^{-3}$ as the density of liquid N_2 at 77 K the porosities of the samples were calculated as a percentage of volume (see Table I). The following values of the true densities of the solids were used: 3.0 $g\,cm^{-3}$ for boehmite, 3.7 $g\,cm^{-3}$ for γ/δ-Al_2O_3 and θ-Al_2O_3 and 4.0 $g\,cm^{-3}$ for α-Al_2O_3 [10].

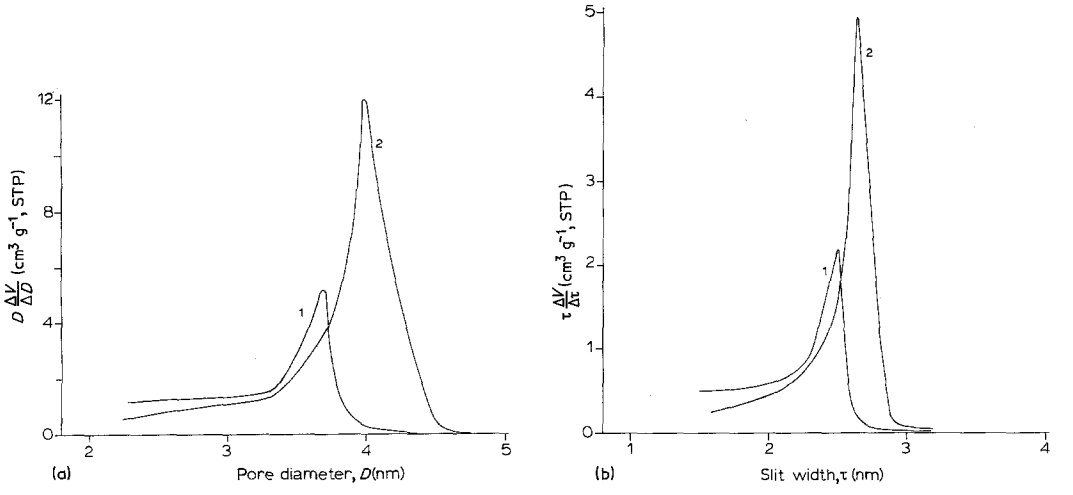

Figure 3 Pore size distribution curves for boehmite membranes (1), and for γ-Al_2O_3 membranes calcined at 400° C (2), assuming (a) cylindrical pores and (b) slit-shaped pores.

TABLE II Microstructural characteristics of gels treated at 500° C, for different amounts of acid in the sol

Mol $HClO_4$ per mol γ-AlOOH	D_{hkl} (average) (nm)	Modal pore size		Porosity (%)
		cylindrical (nm)	slit (nm)	
0.05	3.7	4.1	2.8	49
0.07	4.7	3.8	2.6	44
0.09	3.7	3.7	2.6	42
0.11	3.9	3.5	2.5	38

As shown in Table I, the BET surface area decreases and the pore size increases with increasing temperature, whereas the porosity and the crystallite size are nearly constant and exhibit no systematic change in the range of 400 to 800° C.

3.3. The influence of the acid concentration in the sol on the properties of the calcined gels

A sol was prepared containing 0.05 mol $HClO_4$ per mol boehmite. This sol was divided into 4 parts and samples were prepared containing 0.05, 0.07, 0.09 and 0.11 mol $HClO_4$ per mol boehmite respectively. The membranes prepared from these samples were heated to 500° C. The microstructural characteristics of the samples are presented in Table II. It appears that the crystallite size of the calcined gels shows no systematic change with the acid concentration, whereas both pore size and porosity decrease with increasing acid concentration. Hence, it is most likely that the stacking density of the particles increases with increasing acid concentration. The pore size distribution curve remains very narrow for all samples. This topic is being further investigated and results will be presented later on.

3.4. Membranes on a porous support

A sol containing 0.07 mol HNO_3 per mol boehmite was used for the preparation of supported membranes. The membranes were calcined at 400° C and gas adsorption–desorption measurements were performed. The result is given in Fig. 4, Curve A. Also a pure support was measured (Fig. 4, Curve B) and it appears that about 80% of the surface area of the supported membranes is taken up by the support. The membrane material is responsible for the hysteresis loop of Fig. 4. The modal pore size of the supported membrane can be found by means of the steepest part at which the desorption curve approaches the adsorption isotherm [13]. This point is marked with an arrow in Fig. 4. The modal pore size calculated is 4.0 nm for cylindrical pores and 2.7 nm for slit-shaped pores. This corresponds exactly with the modal pore size obtained for the non-supported membrane calcined at 400° C (see Table I). The porosity of the supported membrane was calculated by the following procedure. The surface area of the pure support was subtracted from that of the supported membrane, giving the surface area of the membrane. When it is assumed that the BET surface area of the supported membrane and the non-supported membrane have the same value (i.e. 301 $m^2 g^{-1}$ according to Table I), the amount of membrane material can be calculated. Subtraction of the adsorbed amount of gas on the pure support at a relative pressure of 0.9 from the amount adsorbed on the supported membranes at the same relative pressure gives the gas adsorption of the pure membrane. Thus the amount of gas adsorbed per unit weight of membrane can be calculated. At this relative pressure all the pores of the membrane are filled with nitrogen, as shown by the absence of hysteresis at and above this pressure. Therefore Gurvitsch's rule (see Section 3.2) can be applied.

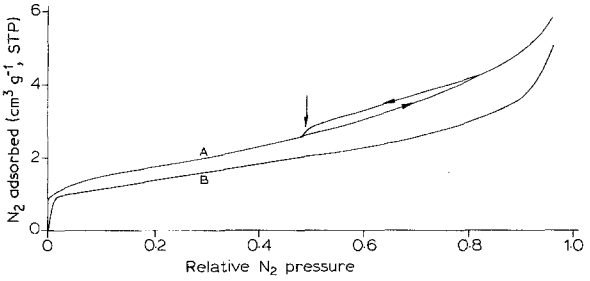

Figure 4 Gas adsorption–desorption measurements of membranes on a porous support (A), and of a pure support (B).

By this procedure a membrane porosity of 60% can be calculated. This corresponds reasonably well with 54% as found for the non-supported membranes, taking into account that the calculation was performed via many steps. It can be concluded that both pore size and porosity of supported membranes, prepared from the same type of sol, corresponds to those of non-supported membranes within the limits of experimental error. Differences between the microstructure of the membranes, if they exist, are small.

4. Discussion

4.1. Formation of the microstructure of the boehmite gel

As shown in Fig. 3 the structures formed are extremely uniform in pore size. In order to understand the causes of this uniformity, the membrane forming mechanism has been studied in more detail. The structure formed primarily is the lyogel at the gelling stage of the sol. During drying this gel shrinks as a result of capillary forces acting on the gel structure. The driving force of the drying process is the H_2O vapour pressure. At equilibrium the Kelvin equation relates the relative vapour pressure (P/P_0) to the pore size of the drying porous solid, according to [13]

$$\ln (P/P_0) = -\frac{2\gamma V}{\tau RT}, \qquad (1)$$

in which γ, V, R and T represent the surface tension of the liquid, the molar volume of the liquid, the gas constant and the absolute temperature respectively. In Equation 1 slit shaped pores with a slit width τ and complete wetting of the solid surface (contact angle of 0°) were assumed. The assumption of slit-shaped pores will be justified in Section 4.2. The thickness of the water film adsorbed on both sides of the slit-shaped pores should be taken into account. Because the calculation serves an illustrative purpose only (see below) the same values were taken as those used for N_2 (see Section 3.2).

TABLE III Pore size (slit width) as a function of the relative H_2O pressure at 20° C at which the pore is emptied and the corresponding capillary pressures

P/P_0	τ (nm)	ΔP (MPa)
0.99	119	1.36
0.90	14	14.2
0.70	5.1	49.0
0.50	3.3	94.0
0.30	2.3	163.0

The capillary pressure (ΔP) acting on the drying porous solid is a function of the capillary size. Again assuming slit-shaped pores and complete wetting of the solid surface, the following form of the well-known equation of Young–Laplace is obtained [13]

$$\Delta P = \frac{2\gamma}{\tau}. \qquad (2)$$

In Table III the sizes of the pores emptied at a given relative H_2O pressure at equilibrium are presented, together with the capillary pressures as a function of these pore sizes. This table shows that the capillary compaction pressures can be very high in finely dispersed systems during drying.

During the initial stage of the drying process a reorganization of the gel structure occurs. This process is illustrated in Fig. 5. Here, a schematic illustration of part of a cross-section of the gel layer is given, which consists of three plate-shaped crystallites oriented parallel to the surface of the gel layer. Crystallite A is in direct contact with the atmosphere, whereas crystallites B and C are situated deeper in the gel layer. The three crystallites are oriented parallel, thereby generating two slit-shaped pores. Fig. 5a represents the start of the drying process when all pores are filled with liquid. When the drying process proceeds water will evaporate from the top of the gel layer and at a

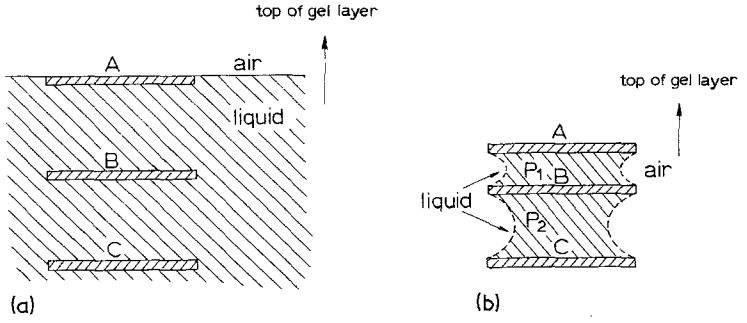

Figure 5 Part of a cross-section of the gel layer at (a) the onset of the drying process, and (b) when the drying process is in progress.

given moment water will be partially replaced by air which results in the situation given in Fig. 5b. Because the H_2O vapour pressure will have the lowest value at the top of the gel layer, the meniscus of the liquid between A and B will be more strongly curved than that between B and C. This gives $P_2 > P_1$ and therefore, crystallite B will be forced in the direction of crystallite A. Hence, smaller pores become smaller and larger pores larger, which would lead to inhomogeneities and ultimately to cracks. However, this process is stopped by the particle repulsion forces resulting from the charged particle surfaces in the walls of pores. The repulsion forces are larger in the smaller pores and counteract the capillary forces. As long as friction forces are not too large the gel structure will relax towards a uniform and densely packed structure. The presence of particle repulsion can be shown by adding water to dried gels. The gels then peptise spontaneously and again form stable sols. Thus, it can be concluded that the uniform ultra-fine structures result from a combined action of capillary compaction forces and particle repulsion.

4.2. Particle shape and size and the resulting shape and size of pores

4.2.1. Boehmite gels

In sols containing very small crystallites, the sol particles are normally formed by aggregates of these crystallites. In a solid structure in which aggregates are present, a so-called bimodal pore size distribution curve is usually obtained, because both small pores within the aggregates and large pores between the aggregates are found (see for example [5]). The pore-size distribution of the dried boehmite membranes, however, shows that there is only one type of pore present. Apparently the aggregates of the boehmite sol, if present, break up during drying as a result of capillary forces. Therefore, the microstructure of the dried boehmite gel can be described completely by the crystallite size and shape and by the way these crystallites are stacked.

An average crystal size can be calculated from the specific surface area of the boehmite sample. It is known, however, that the specific surface area measured by the BET method differs from the geometric surface area when micropores are present [13]. The influence of micropores can be evaluated by using the adsorption data of Lippens

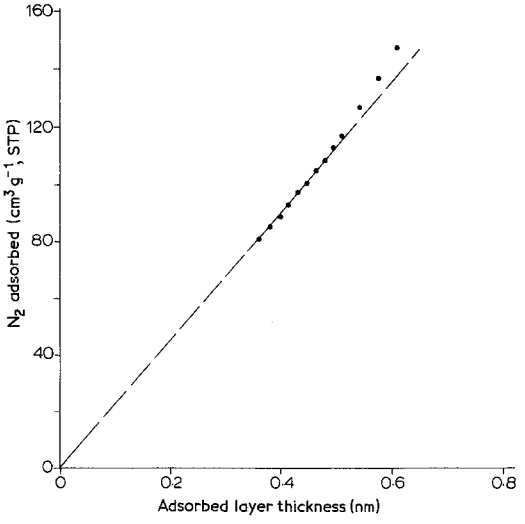

Figure 6 Gas adsorption as a function of the adsorbed layer thickness for a boehmite sample prepared by coagulation in butanol.

which are obtained from aluminium hydroxides and oxides without micropores [8, 14]. From these data Lippens calculated the adsorbed layer thickness as a function of the relative pressure, for relative pressures above 0.08. When the adsorbed amount of nitrogen of an arbitrarily chosen sample is plotted as a function of this adsorbed layer thickness, it can be concluded that the influence of micropores is absent when the extrapolated curve passes through the origin. Applying this procedure to our boehmite sample shows that micropores are present. Therefore, another sample was prepared from the same boehmite sol by coagulating this sol in butanol and drying the gel product formed.* The gas adsorption data of this sample are shown in Fig. 6. The extrapolated initial part of the curve passes through the origin. The upward deviation from the straight line at relative thick adsorbed layers is a result of vapour condensation. The BET surface area of this sample is $359 \pm 4\ m^2\ g^{-1}$, instead of a BET surface area of $315\ m^2\ g^{-1}$ of the sample with micropores. With this result an average crystallite size is calculated (see below).

The shape and size of the crystallites was studied by TEM. The results are shown in Fig. 7. When these photographs are used to determine the shape of the boehmite crystallites, it seems that two different types of crystals are present. Fig. 7a clearly represents plate shaped crystallites. However, the sol is mainly (>90%) composed of crystallites

*The surface tension of butanol is a factor three lower than that of water.

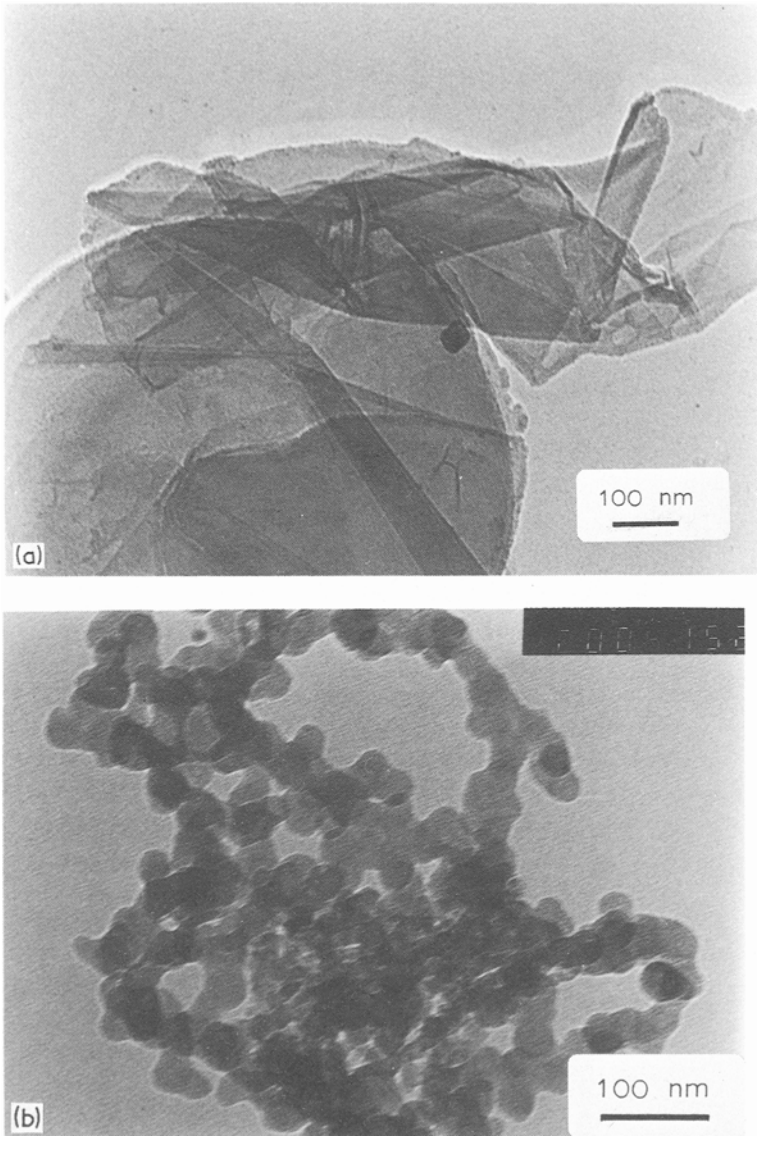

Figure 7 TEM photo of a boehmite sol, showing (a) plate-shaped crystallites, and (b) crystallites with rounded forms.

shown in Fig. 7b, which *seem* to be spherically shaped. The following argument strongly supports the case that the shape of the crystallites in Fig. 7b is nevertheless plate-like.

1. Taking $359\,m^2\,g^{-1}$ as the surface area of boehmite and assuming spherical particles and a totally accessible surface of the crystallites, a crystallite cross-section of 5.7 nm can be calculated. For other shapes, the size in at least one direction through the crystallites has to be less than 5.7 nm, to obtain the surface area measured. The TEM measurements, however, give a particle size of about 25 nm (see Fig. 7b). Therefore, the crystallites have to be anisometrically shaped. The lateral size of the crystallites, as observed by TEM is about 25 nm and the thickness has to be less than 5.7 nm. If plate-shaped particles with a circular cross-section of 25 nm are present, a plate thickness of 2.3 nm can be calculated. Hence, the crystallites at least must have a shape which resembles the plate shape closely.

2. If spherical crystallites of 25 nm are present, a regular stacking with a porosity of 41% would result in a structure in which the narrowest passage is about 10 nm [15]. This is significantly larger than the modal pore size obtained by assuming cylindrical pores (see Fig. 3) and therefore, the particles have to be anisometrically shaped.

3. X-ray line broadening measurements yield 5.5 nm as the average value of the boehmite crystal

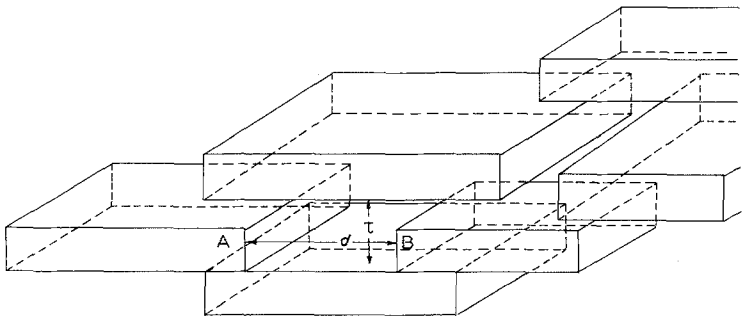

Figure 8 Idealized model of the boehmite membrane microstructure.

size. This is much smaller than the value obtained by TEM and this can be explained by the occurrence of anisometric crystallites (see below).

4. The plate shape is also supported by Fig. 7. If there should be a variation of the thickness within the crystallites, then contrast differences within the crystals would also be present. However, these are not observed.

5. Plate-shaped boehmite crystallites are often found [8], as a consequence of the boehmite lattice that consists of relatively weakly bonded layers.

Accepting plate-shaped boehmite crystallites, a regular particle stacking without large pores can only be obtained in a so-called card-pack structure, in which the large planes of the plates are more or less parallel to one another, this results in slit-shaped pores. A drawing of the idealized microstructure is given in Fig. 8. Because of the relatively high stacking density of the boehmite crystallites, the plate thickness and the slit width should be about the same. The plate-shaped boehmite crystals have their *b*-axis perpendicular to the large planes of the plates [8, 11]. Taking the ASTM lattice constants for boehmite, the plate thickness can be calculated now by multiplying the D_{120} and D_{031} crystallite size by 0.512 and 0.576 respectively. A crystal thickness of 3.2 nm from D_{120} and of 2.8 nm from D_{031} is obtained by this method. These results indeed show that there is a reasonable agreement between the slit width of 2.5 nm as measured from desorption measurements (Fig. 3b) and the calculated plate thickness here. Furthermore, the integral intensity of the [0 2 0] reflection compared with the [1 2 0] and [0 3 1] reflections, is about 10 times higher than can be expected for a random distribution of crystal directions, as obtained from the ASTM data for boehmite. A card-pack structure of plates according to Fig. 8, in which the *b*-axis is perpendicular to these plates, gives rise to such a texture and this explains the observed X-ray intensity ratios qualitatively.

To support the concept of plate-shaped crystals stacked in a card-pack structure, a sol was prepared clearly containing plate-shaped crystallites only. This was done by treating a sol with 0.07 mol HNO_3 per mol of boehmite for 5 h in an autoclave at 200° C. A TEM photograph of this sol is given in Fig. 9. The crystal size measured is 14.5 nm for D_{120}, 12.3 nm for D_{031} and 6.4 nm for D_{080} and calculating the crystal thickness according to the procedure described above gives 7.4, 7.1 and 6.4, respectively (see Table I). The modal slit width obtained from gas adsorption–gas desorption measurements is 5.6 nm, which is reasonably close to the average plate thickness of 7.0 nm.

Summarizing, we can conclude that a consistent explanation of the experimental results can be presented by describing the microstructure of dried boehmite membranes as plate-shaped particles stacked in a card-pack structure. This close-packed structure is the result of gel-compaction due to capillary forces during water extraction in the drying step.

4.2.2. The calcined aluminas

So far the discussion has been limited to the microstructure of the boehmite membranes. The point to be discussed now is to what extent the microstructure is affected by the transition:

$$2\gamma\text{-AlOOH} \rightarrow \gamma\text{-}Al_2O_3 + H_2O \qquad (3)$$

According to the literature the decomposition process of boehmite depends on the boehmite crystal size. For large boehmite crystals, the transition is known to proceed via a pseudomorphic process. The γ-Al_2O_3 crystallites are then formed within the γ-AlOOH crystal, thereby creating new pores and increasing the surface area [8, 10]. When very small crystallites are taken, however, no new pores

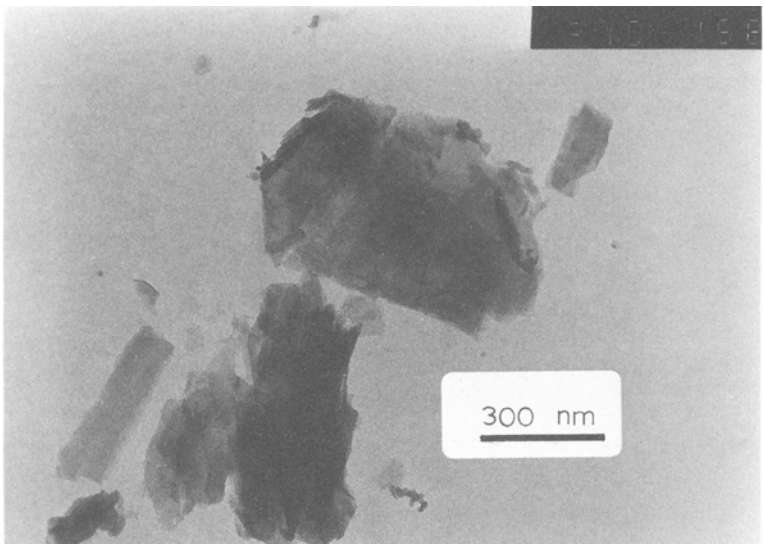

Figure 9 TEM photograph of a boehmite sol prepared by autoclave treatment at 200° C.

are formed and the specific surface area decreases [8]. The specific surface area and the pore size are then determined by the size and shape of the boehmite crystallites and by the way these crystallites are stacked. This structure would then be relatively unaffected by the transition. In our case the transition is not accompanied by the development of a new class of pores and a significant increase of the surface area. This strongly points to the second transition mechanism.

In Fig. 10 TEM photos are given of a sample which is successively calcined at 400° C and powdered. The same crystallites are shown in bright field (Fig. 10a) and in dark field, taking only a part of a diffraction ring (Fig. 10b). When Fig. 10a is compared with the boehmite crystals shown in Fig. 7b it appears that the outer shapes of the former crystal-clusters of boehmite are clearly visible in Fig. 10a. The observation that the outer shape of the boehmite crystals remains unchanged by the transition into γ-Al_2O_3 is another argument that the basic structure of the boehmite membranes remains intact. In Fig. 10b every bright spot represents one crystallite of γ-alumina. These γ-Al_2O_3 crystallites are so small that more than one γ-Al_2O_3 crystallite must be formed within one boehmite crystal. Apparently, no pores are formed between those γ-Al_2O_3 crystallites which are situated within one former boehmite crystal, as no increase of the surface area is observed. During the decomposition process the boehmite crystals have to shrink, because H_2O is expelled, the true density of the material increases and no pores are formed within the boehmite crystals.

As shown in Table I, the porosity of the membranes increases during the transition of boehmite into the oxidic phase. Taking 41% as the porosity of the boehmite membrane and using Equation 3 and the true densities of boehmite and γ-Al_2O_3, the porosity of γ-Al_2O_3 can be calculated to be 59%, when it is assumed that the decomposition is not accompanied by a macroscopic shrinkage of the membrane. This figure is significantly higher than the measured porosity of 54%. The membranes form no cracks during the transition. Hence, no macroscopic shrinkage occurs in the lateral dimensions of the membrane and the transition should be accompanied by some decrease of the membrane thickness.

In Fig. 8, a mechanism is proposed for the transition of boehmite into γ-Al_2O_3, which fits with most observations. The boehmite crystallites A and B shrink during their decomposition. If it is assumed that their centres of mass remain in place, then from Fig. 8 it can be seen that no macroscopic shrinkage occurs in the lateral dimensions and that the value of d increases. As a result the porosity increases whereas the slit width, τ, remains unaffected. However, a small increase of τ is observed experimentally. This can be explained by taking into account the sintering process which will accompany the decomposition of boehmite. Table IV shows that pore growth occurs during sintering at 400° C. If the centres of mass of the boehmite crystals remain in place during the transition of boehmite, as

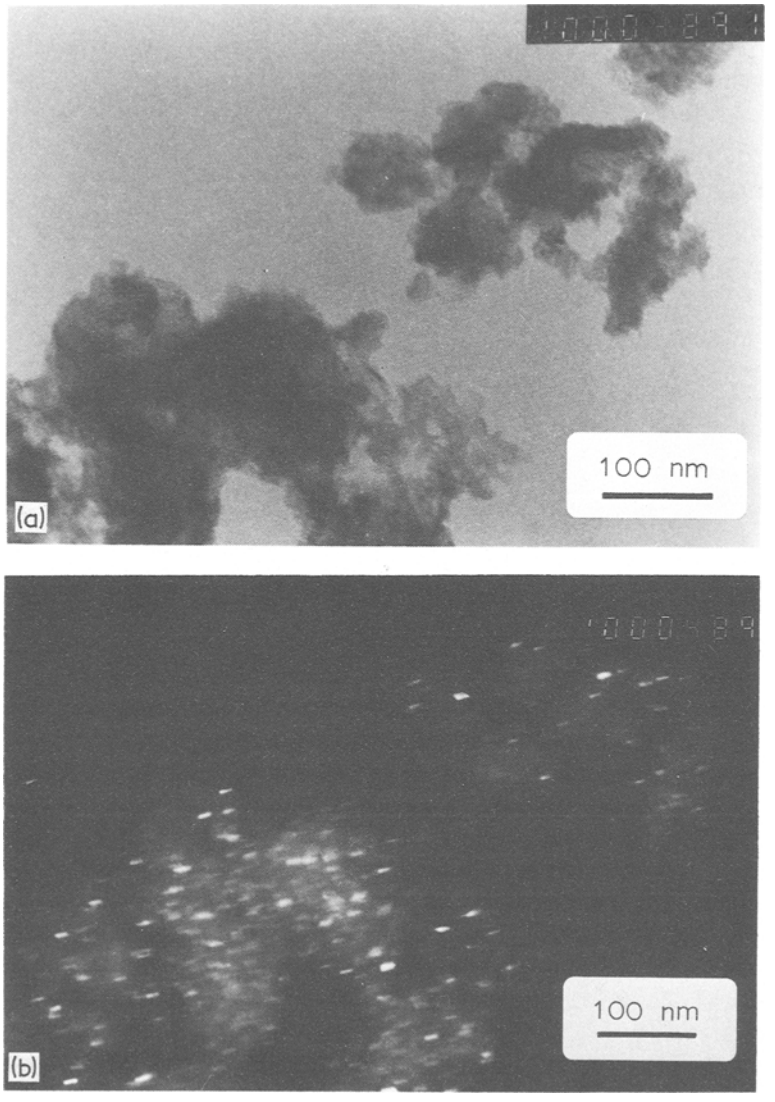

Figure 10 TEM photographs of an alumina sample calcined at 400° C. (a) Bright-field, and (b) dark-field, showing the individual alumina crystallites.

TABLE IV The influence of prolonged heat treatment on surface area, pore size and porosity

Temperature (° C)	Time (h)	BET surface ($m^2 g^{-1}$)	Pore size (nm)		Porosity (%)
			Cylindrical shape	Slit-shape	
400	34	301 ± 7	4.0	2.7	53
400	170	276 ± 4	4.4	2.9	53
400	850	249 ± 2	4.9	3.1	53
705	5	207 ± 2	4.9	3.2	51
705	25	178 ± 2	5.6	3.6	51
705	123	159 ± 2	6.1	3.8	51
705	433	149 ± 3	6.7	4.2	51
705	933	148 ± 2	6.9	4.3	51

suggested above, the crystal surfaces should glide along one another. This implies a plastic deformation of the structure. After the transition no plastic deformation can occur, because the structure is brittle then and deformation will cause cracking.

4.3. The sintering process

Prolonged heat treatment at $T \geqslant 400^\circ$C results in a moderate increase of the modal pore size (Table IV). The pore size distribution curve remains narrow and the porosity is not affected by this treatment. To avoid sintering processes of the membranes during their long-term use, a pretreatment of the membrane material at a temperature higher than the temperature at which the membrane is used will probably be sufficient.

Table I gives the properties of the membranes as a function of temperature. Because heating was performed at a rate of 10° C per hour and the samples were held 34 h at the temperatures given in this table, the effect of time is also included. However, it can be concluded from Table IV that differences in sintering time of the samples of Table I have only a slight effect on the microstructure of these samples.

As shown in Table I the surface area decreases and the pore size increases with increasing temperature, whereas both the crystal size and the porosity remain constant to 800° C. This indicates that the dominant sintering mechanism is surface diffusion. The decrease of the surface area can therefore be attributed to the disappearance of the smallest pores only. More experiments in this temperature region will be carried out and the results presented later.

5. Conclusions

1. The preparation and characterization of thin alumina membranes with a modal pore size of 2.7 nm, a porosity of about 50% and a narrow pore size distribution has been described.

2. The pore size of the alumina membranes can be tailor made, by varying the sintering temperature and/or the acid concentration of the sol.

3. The formation of a system with a narrow pore size distribution can be explained in terms of capillary compaction forces and repulsion forces between the crystallites.

4. A consistent explanation of the microstructural parameters of the dried boehmite membrane can be given on the basis of a card-pack stacking of plate-shaped crystallites. This results in slit-shaped pores.

5. The microstructure of the alumina formed from boehmite by calcination is closely related to that of the preceding boehmite structure.

6. It is most likely that the sintering mechanism in the temperature range of 400 to 800° C is surface diffusion.

Acknowledgements

Mrs S. M. Nijhuis is acknowledged for technical assistance and Dr J. Beyer is thanked for his help with the TEM experiments. Financial assistance from the Ministries of Science Affairs and Economical Affairs is acknowledged.

References

1. H. K. LONSDALE, *J. Membrane Sci.* **10** (1982) 81.
2. A. F. M. LEENAARS, K. KEIZER and A. J. BURGGRAAF, "Separation with Inorganic Membranes", (Laboratory of Inorganic Materials Science, Twente University of Technology, Enschede, The Netherlands (in Dutch)).
3. M. A. C. G. VAN DE GRAAF, T. VAN DIJK, M. A. DE JONGH and A. J. BURGGRAAF, in "Proceedings of the Ninth International Conference on Science of Ceramics", Noordwijkerhout, November 1977, edited by K. J. de Vries (The Nederlandse Keramische Vereniging, Enschede, 1977) p. 75.
4. M. A. C. G. VAN DE GRAAF, K. KEIZER and A. J. BURGGRAAF, in "Proceedings of the Tenth International Conference on Science of Ceramics", Berchtesgaden, September 1979, edited by H. Hausner (Deutsche Keramische Gesellschaft, Berlin, 1980) p. 83.
5. M. A. C. G. VAN DE GRAAF, J. H. H. TER MAAT and A. J. BURGGRAAF, in "Ceramic Powders", edited by P. Vincenzini (Elsevier Scientific Publishing Company, Amsterdam, 1983) p. 783.
6. B. E. YOLDAS, *Ceram. Bull.* **54** (1975) 286.
7. B. E. YOLDAS, *J. Mater. Sci.* **10** (1975) 1856.
8. B. C. LIPPENS, Thesis, Delft University of Technology, The Netherlands (1961).
9. S. J. WILSON, J. D. C. McCONNELL and M. H. STACEY, *J. Mater. Sci.* **15** (1980) 3081.
10. S. J. WILSON and M. H. STACEY, *J. Coll. Interf. Sci.* **82** (1981) 507.
11. S. J. WILSON, *J. Solid State Chem.* **30** (1979) 247.
12. H. P. KLUG and L. E. ALEXANDER, "X-ray Diffraction Procedures for Polycrystalline and Amorphous Materials", 2nd edn (Wiley and Sons, New York, 1974) Chap. 9.
13. S. J. GREGG and K. S. W. SING, "Adsorption, Surface Area and Porosity" (Academic Press, London and New York, 1967) Chap. 3.
14. B. C. LIPPENS, B. G. LINSEN and J. H. DE BOER, *J. Catal.* **3** (1964) 32.
15. S. KRUYER, *Trans. Farad. Soc.* **54** (1958) 1758.

Received 24 May
and accepted 24 June 1983